Article

New n-Type Organic Semiconductors: Synthesis, Single Crystal Structures, Cyclic Voltammetry, Photophysics, Electron Transport, and Electroluminescence of a Series of Diphenylanthrazolines

Christopher J. Tonzola, Maksudul M. Alam, Werner Kaminsky, and Samson A. Jenekhe

J. Am. Chem. Soc., **2003**, 125 (44), 13548-13558• DOI: 10.1021/ja036314e • Publication Date (Web): 10 October 2003

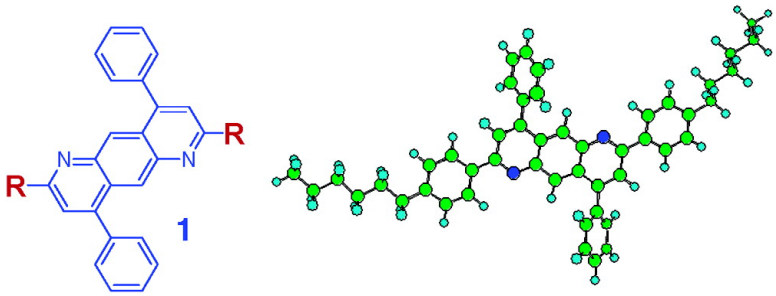

More About This Article

Additional resources and features associated with this article are available within the HTML version:

- Supporting Information
- Links to the 20 articles that cite this article, as of the time of this article download
- Access to high resolution figures
- Links to articles and content related to this article
- Copyright permission to reproduce figures and/or text from this article

View the Full Text HTML

J|A|C|S
ARTICLES
Published on Web 10/10/2003

New n-Type Organic Semiconductors: Synthesis, Single Crystal Structures, Cyclic Voltammetry, Photophysics, Electron Transport, and Electroluminescence of a Series of Diphenylanthrazolines

Christopher J. Tonzola,[†] Maksudul M. Alam,[‡] Werner Kaminsky,[†] and Samson A. Jenekhe*,[†,‡]

Contribution from the Department of Chemistry and Department of Chemical Engineering, University of Washington, Seattle, Washington 98195-1750

Received May 23, 2003; E-mail: jenekhe@cheme.washington.edu

Abstract: The synthesis, properties, and electroluminescent device applications of a series of five new diphenylanthrazoline molecules **1a**−**1e** are reported. Compounds **1b**, **1c**, and **1d** crystallized in the monoclinic system with the space groups $P2_1/c$, $C2/c$, and $P2_1/c$, respectively, revealing highly planar molecules. Diphenylanthrazolines **1a**−**1e** have a formal reduction potential in the range −1.39 to −1.58 V (versus SCE) and estimated electron affinities (LUMO levels) of 2.90−3.10 eV. Compounds **1a**−**1e** emit blue light with fluorescence quantum yields of 58−76% in dilute solution, whereas they emit yellow-green light as thin films. The diphenylanthrazoline molecules as the emissive layers in light-emitting diodes gave yellow light with a maximum brightness of 133 cd/m^2 and an external quantum efficiency of up to 0.07% in ambient air. Bilayer light-emitting diodes using compounds **1a**−**1e** as the electron-transport layer and poly-(2-methoxy-5-(2′-ethyl-hexyloxy)-1,4-phenylene vinylene) as the emissive layer had a maximum external efficiency of 3.1% and 2.0 lm/W and a brightness of up to 965 cd/m^2 in ambient air. These results represent enhancements of up to 50 times in external quantum efficiency and 17 times in brightness when using **1a**−**1e** as the electron-transport materials in polymer light-emitting diodes. These results demonstrate that the new diphenylanthrazolines are promising n-type semiconductors for organic electronics.

Introduction

Organic semiconductors and conjugated polymers are of wide current interest for applications in electronic and optoelectronic devices including light-emitting diodes,[1−4] thin film transistors,[5,6] and photovoltaic cells.[7,8] The vast majority of synthetic effort and structure−property studies in the field have to date been devoted to organic and polymeric semiconductors having p-type (electron donor, hole transport) properties.[1e,2a,3,9] n-Type (electron acceptor, electron transport) organic and polymer semiconductors are also needed for developing more efficient and high performance light-emitting diodes (LEDs), photovoltaic cells, and other building blocks of plastic electronics. In this paper, we report the synthesis, detailed structural characterization, and investigation of the electrochemical, photophysical, electron transport, and light-emitting device properties of a series

[†] Department of Chemistry.
[‡] Department of Chemical Engineering.

(1) (a) Tang, C. W.; Van Slyke, S. A. *Appl. Phys. Lett.* **1987**, *51*, 913−915. (b) Kolosov, S.; Adamovich, V.; Djurovich, P.; Thompson, M. E.; Adachi, C. *J. Am. Chem. Soc.* **2002**, *124*, 9945−9954. (c) Baldo, M. A.; O'Brien, D. F.; You, Y.; Shoustikov, A.; Sibley, S.; Thompson, M. E.; Forrest, S. R. *Nature* **1998**, *395*, 151−154. (d) Shirota, Y.; Kinoshita, M.; Noda, T.; Okumoto, K.; Ohara, T. *J. Am. Chem. Soc.* **2000**, *122*, 11021−11022. (e) Mitschke, U.; Bauerle, P. *J. Mater. Chem.* **2000**, *10*, 1471−1507.
(2) (a) Kraft, A.; Grimsdale, A. C.; Holmes, A. B. *Angew. Chem., Int. Ed.* **1998**, *37*, 402−428. (b) Bernius, M. T.; Inbasekaran, M.; O'Brien, J.; Wu, W. *Adv. Mater.* **2000**, *12*, 1737−1750. (c) Bao, Z.; Rogers, J. A.; Dodabalapur, A.; Lovinger, A. J.; Katz, H. E.; Raju, V. R.; Peng, Z.; Galvin, M. E. *Opt. Mater.* **1999**, *12*, 177−182. (c) Cao, Y.; Parker, D.; Yu, G.; Zhang, C.; Heeger, A. J. *Nature* **1999**, *397*, 414−417.(d) Friend, R. H.; Gymer, R. W.; Holmes, A. B.; Burroughes, J. H.; Marks, R. N.; Taliani, C.; Bradley, D. C. C.; dos Santos, D. A.; Bredas, J. L.; Loglund, M.; Salaneck, W. R. *Nature* **1999**, *397*, 121−128.
(3) (a) Zheng, M.; Ding, L.; Gürel, E. E.; Karasz, F. E. *J. Polym. Sci., Part A: Polym. Chem.* **2002**, *40*, 235−241. (b) Peng, Z.; Bao, Z.; Galvin, M. E. *Adv. Mater.* **1998**, *10*, 680−684. (c) Chen, J. P.; Markiewicz, D.; Lee, V. Y.; Klaerner, G.; Miller, R. D.; Scott, J. C. *Synth. Met.* **1999**, *107*, 203−207. (d) Robinson, M. R.; Wang, S.; Bazan, G. C.; Cao, Y. *Adv. Mater.* **2000**, *12*, 1701−1704.
(4) (a) Tarkka, R. M.; Zhang, X.; Jenekhe, S. A. *J. Am. Chem. Soc.* **1996**, *118*, 9438−9439. (b) Jenekhe, S. A.; Zhang, X.; Chen, X. L.; Choong, V.-E.; Gao, Y.; Hsieh, B. R. *Chem. Mater.* **1997**, *9*, 409−412. (c) Zhang, X.; Shetty, A. S.; Jenekhe, S. A. *Macromolecules* **1999**, *32*, 7422−7429. (d) Cui, Y.; Zhang, X.; Jenekhe, S. A. *Macromolecules* **1999**, *32*, 3824−3826. (e) Zhang, X.; Jenekhe, S. A. *Macromolecules* **2000**, *33*, 2069−2082. (f) Tonzola, C. J.; Alam, M. M.; Jenekhe, S. A. *Adv. Mater.* **2002**, *14*, 1086−1090. (g) Zhang, X.; Kale, D. M.; Jenekhe, S. A. *Macromolecules* **2002**, *35*, 382−393. (h) Alam, M. M.; Jenekhe, S. A. *Chem. Mater.* **2002**, *14*, 4775−1780. (i) Alam, M. M.; Tonzola, C. J.; Jenekhe, S. A. *Macromolecules* **2003**, *36*, 6577−6587.
(5) (a) Katz, H. E.; Bao, Z. *J. Phys. Chem. B* **2000**, *104*, 671−678. (b) Katz, H. E.; Bao, Z.; Gilat, S. L. *Acc. Chem. Res.* **2001**, *14*, 359−369. (c) Dimitrakopoulos, C. D.; Malenfant, P. R. L. *Adv. Mater.* **2002**, *14*, 99−117. (d) Horowitz, G. *Adv. Mater.* **1998**, *10*, 365−377. (e) Sirringhaus, H.; Tessler, N.; Friend, R. H. *Science* **1998**, *280*, 1741−1744.
(6) (a) Babel, A.; Jenekhe, S. A. *Adv. Mater.* **2002**, *14*, 371−374. (b) Babel, A.; Jenekhe, S. A. *J. Phys. Chem. B* **2002**, *106*, 6129−6132. (c) Babel, A.; Jenekhe, S. A. *J. Phys. Chem. B* **2003**, *107*, 1749−1754.
(7) (a) Brabec, C. J.; Sariciftci, N. S.; Hummelen, J. C. *Adv. Funct. Mater.* **2001**, *11*, 15−26. (b) Yu, G.; Gao, J.; Hummelen, J. C.; Wudl, F.; Heeger, A. J. *Science* **1995**, *267*, 1969−1971.
(8) (a) Antoniadis, H.; Hsieh, B. R.; Abkowitz, M. A.; Jenekhe, S. A.; Stolka, M. *Synth. Met.* **1994**, *62*, 265−271. (b) Jenekhe, S. A.; Yi, S. *Appl. Phys. Lett.* **2000**, *77*, 2635−2637.
(9) *Electronics Materials: The Oligomer Approach;* Muellen, K., Wegner, G., Eds.; Wiley VCH: Weinheim, Germany, 1998.

10.1021/ja036314e CCC: $25.00

Chart 1

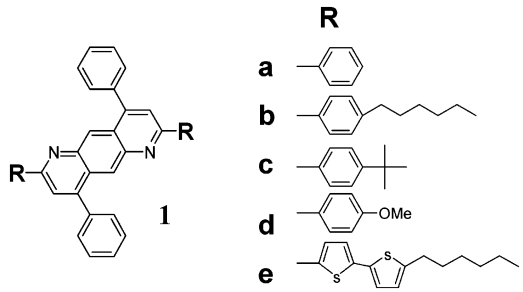

of five new n-type organic semiconductors based on 4,9-diphenylanthrazoline **1**: 2,7-bis(phenyl)-4,9-diphenylanthrazoline (**1a**), 2,7-bis(4′-*n*-hexylphenyl)-4,9-diphenylanthrazoline (**1b**), 2,7-bis(4′-*tert*-butylphenyl)-4,9-diphenylanthrazoline (**1c**), 2,7-bis(4′-methoxyphenyl)-4,9-diphenylanthrazoline (**1d**), and 2,7-bis(5′-*n*-hexyl-2,2′-bithiophene)-4,9-diphenylanthrazoline (**1e**) (Chart 1).

Surprisingly, only a limited number of molecular building blocks have been explored as electron-transport (n-type) materials for organic electronics.[5−10] Electron transport has been observed in fluorinated oligothiophenes,[11] perfluorinated oligophenylenes,[12] fluorinated phthalocyanines,[13] naphthalene and perylene diimides,[14] and silole compounds.[15] In the case of organic and polymer LEDs, aluminum quinolate (Alq_3),[16] oxadiazole molecules and polymers,[3b,10,17] benzimidazoles,[18] quinoxalines and polyquinoxalines,[4d,19] polypyridines,[20] and polyquinolines[4,21] have been used as electron-transport materials to varied degrees of success in improving device performance.

The molecular structures and half-wave reduction potentials ($E_{1/2}$ vs SCE) of a series of aromatic heterocycles and hydrocarbons are shown in Chart 2.[22−25] Because the electron affinity (EA) and ionization potential (IP) that define the HOMO/LUMO levels of aromatic molecules are well correlated with electrochemical reduction and oxidation potentials,[22] the structure-reduction-potential trends in Chart 2 provide a first-level basis for selecting target new n-type molecules for synthesis and investigation. Heteroaromatic rings containing only imine nitrogen atoms (C═N) generally have a less negative reduction potential compared to analogous aromatic hydrocarbons and heteroaromatic rings containing oxygen or sulfur atoms. Among polycyclic rings, linear expansion is most beneficial to increasing the reduction potential. Although oxadiazole (X), benzothiadiazole (IX), and quinoline (III) are most commonly used as building blocks for increasing the reduction potential and electron affinity of current electron-transport materials for LEDs,[3b,4,10,17] anthracene derivatives such as acridine (V), phenazine (VI), and 1,4,5,8,-tetraazaanthracene or pyrazinoquinoxaline (VII) are potentially superior. The synthetically readily accessible anthracene derivatives, diphenylanthrazolines **1**, were therefore selected for initial investigation as new n-type semiconductors for organic electronics.

Chart 2. Structure and Half-Wave ($E_{1/2}$) Reduction Potentials (vs SCE) of Aromatic Hydrocarbons and Heterocycles[a]

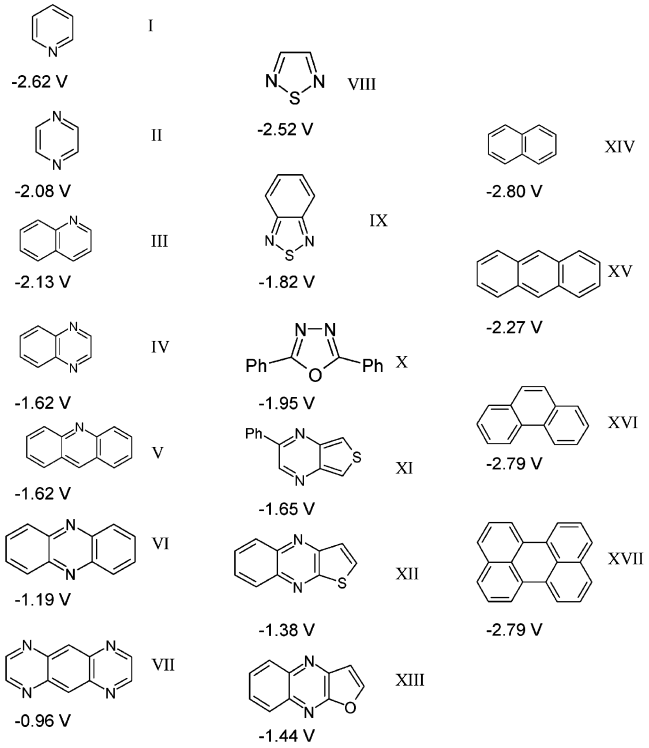

[a] For $E_{1/2}$ data, see refs 22−25.

Results and Discussion

Synthesis and Characterization. Scheme 1 outlines the synthesis of the series of diphenylanthrazolines. The acid-catalyzed Friedlander condensation reactions[26,27] yielded the desired products in 62−78% yields. The diphenyl phosphate (DPP) catalyst was readily removed by precipitation into a 10%

(10) Strukelj, M.; Papadimitrakopoulos, F.; Miller, T. M.; Rothberg, L. J. *Science* **1995**, *67*, 1969−1972.
(11) (a) Fachetti, A.; Mushrush, M.; Katz, H. E.; Marks, T. J. *Adv. Mater.* **2003**, *15*, 33−38. (b) Sakamoto, Y.; Shingo, K.; Suzuki, T. *J. Am. Chem. Soc.* **2001**, *123*, 4643−4644. (c) Fachetti, A.; Deng, Y.; Wang, A.; Koide, Y.; Sirringhaus, H.; Marks, T. J.; Friend, R. H. *Angew. Chem., Int. Ed.* **2000**, *39*, 4547−4551.
(12) Sakamoto, Y.; Suzuki, T.; Miura, A.; Fujikawa, H.; Tokito, S.; Taga, Y. *J. Am. Chem. Soc.* **2000**, *122*, 1832−1833.
(13) Bao, Z.; Lovinger, A. J.; Brown, J. *J. Am. Chem. Soc.* **1998**, *120*, 207−208.
(14) (a) Katz, H. E.; Lovinger, A. J.; Johnson, J.; Kloc, C.; Siegrist, T.; Li, W.; Lin, Y.-Y.; Dodabalapur, A. *Nature* **2000**, *404*, 478−481. (b) Gregg, B. A.; Cormier, R. A. *J. Am. Chem. Soc.* **2001**, *123*, 7959−7960.
(15) Murata, H.; Malliaras, G. G.; Uchida, M.; Shen, Y.; Kafafi, Z. H. *Chem. Phys. Lett.* **2001**, *339*, 161−166.
(16) Burrows, P. E.; Shen, Z.; Bulovic, V.; McCarty, D. M.; Forrest, S. R.; Cronin, J. A.; Thompson, M. E. *J. Appl. Phys.* **1996**, *79*, 7991−8006.
(17) (a) Wang, C.; Jung, G. Y.; Hua, Y.; Pearson, C.; Bryce, M. R.; Petty, M. C.; Batsanov, A. S.; Goeta, A. E.; Howard, J. A. K. *Chem. Mater.* **2001**, *13*, 1167−1173. (b) Brown, A. R.; Bradley, D. D. C.; Burroughs, J. H.; Friend, R. H.; Greenham, N. C.; Burn, P. L.; Holmes, A. B.; Kraft, A. *Appl. Phys. Lett.* **1992**, *61*, 2793−2795.
(18) (a) Gao, Z. Q.; Lee, C. S.; Bello, I.; Lee, S. T.; Chen, R. M.; Luh, T. Y.; Shi, J.; Tang, C. W. *Appl. Phys. Lett.* **1999**, *74*, 865−867. (b) Gao, Z. Q.; Lee, C. S.; Bello, I.; Lee, S. T.; Wu, S. K.; Yan, Z. L.; Zhang, X. H. *Synth. Met.* **1999**, *105*, 141−144.
(19) (a) Thomas, K. R. J.; Lin, J. T.; Tao, Y. T.; Chuen, C. H. *Chem. Mater.* **2002**, *14*, 2796−2802. (b) Jandke, M.; Strohriegl, P.; Berleb, S.; Werner, E.; Brütting, W. *Macromolecules* **1998**, *31*, 6434−6443.
(20) (a) Onoda, M.; MacDiarmid, A. G. *Synth. Met.* **1997**, *91*, 307−309. (b) Wang, Y. Z.; Gebler, D. D.; Fu, D. K.; Swager, T. M.; MacDiarmid, A. G.; Epstein, A. J. *Synth. Met.* **1997**, *85*, 1179−1182. (c) Dailey, C. S.; Halim, M.; Rebourt, E.; Horburgh, L. E.; Samuel, I. D. W.; Monkman, A. P. *J. Phys.: Condens. Matter* **1998**, *10*, 5171−5178.
(21) Kim, D. Y.; Lee, S. K.; Kim, J. L.; Kim, J. K.; Lee, H.; Cho, H. N.; Hong, S. I.; Kim, C. Y. *Synth. Met.* **2001**, *121*, 1707−1708.
(22) Parker, V. D. *J. Am. Chem. Soc.* **1976**, *98*, 98−103.
(23) *Encyclopedia of Electrochemistry of the Elements;* Bard, A. J., Lund, H., Eds.; Marcel Dekker: New York, 1984; Vol. XV, pp 168−280.
(24) Armand, J.; Bellec, C.; Boulares, L.; Chaquin, P.; Masure, D.; Pinson, J. *J. Org. Chem.* **1991**, *56*, 4840−4845.
(25) Kobayashi, T.; Kobayashi, S. *Eur. J. Org. Chem.* **2002**, 2066−2073.
(26) *Organic Reactions*; Dauben, W. G., Ed.; Wiley and Sons: New York, 1982; Vol. 28, pp 38−55.
(27) (a) Agrawal, A. K.; Jenekhe, S. A. *Macromolecules* **1991**, *24*, 6806−6808. (b) Agrawal, A. K.; Jenekhe, S. A. *Macromolecules* **1993**, *26*, 895−905. (c) Agrawal, A. K.; Jenekhe, S. A. *Chem. Mater.* **1993**, *5*, 633−640.

Scheme 1 [a]

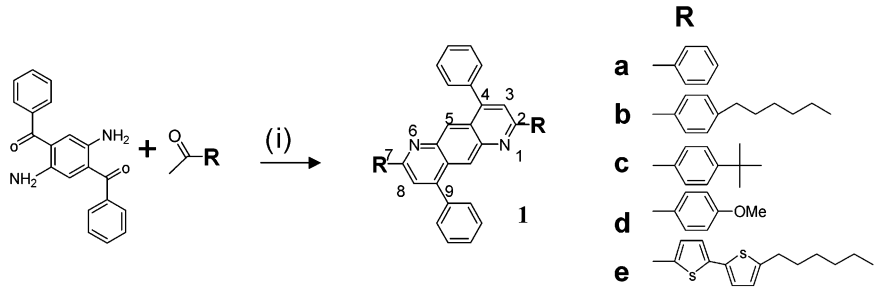

[a] (*i*) Diphenyl phosphate, 140 °C, 24 h.

Table 1. Physical Properties of Diphenylanthrazolines

compd	T_m (°C)	T_D (°C)	λ^{Abs}_{max} (soln) (nm)	ϵ (10^4 M^{-1} cm^{-1})	λ^{Abs}_{max} (film) (nm)	E_g (opt) (eV)	λ^{Em}_{max} (soln) (nm)	λ^{Em}_{max} (film) (nm)	ϕ_f (soln)	ϕ_f (film)
1a	380	406	399	35.2	414	2.70	474	542	0.68	n/a
1b	274	451	395	1.46	409	2.65	482	545	0.70	0.23
1c	356	402	400	9.10	404	2.69	476	527	0.76	0.30
1d	347	420	411	3.51	417	2.64	462	537	0.74	0.28
1e	268	447	488	7.00	514	2.21	524	604	0.58	0.03

triethylamine/ethanol solution. The materials were passed through silica gel columns via flash chromatography to remove insoluble byproducts. They were subsequently recrystallized twice in THF/methanol mixtures ranging from 5 to 20% methanol. Compounds **1b**, **c**, and **d** were obtained as yellow needles, **1a** was obtained as small orange crystals, and **1e** was obtained as red crystalline powder. ^{1}H NMR spectra, FTIR spectra, and mass spectrometry on all products confirm the proposed structures. ^{13}C NMR spectra of some of the compounds (**1b**, **1c**, and **1d**) provided additional confirmation of structure.

All the diphenylanthrazolines were soluble in organic solvents in varying degrees. Compounds **1b**, **1c**, and **1d** were soluble in $CHCl_3$, tetrahydrofuran, and toluene. The decrease in solubility of **1a** and **1e** hindered the solution processing of these materials and made their ^{13}C NMR spectra unattainable. However, thin films of **1a** and **1e** can be solution cast and spin-coated from a $CHCl_3$ solution containing a trace amount of formic acid, respectively. Thin films of all of the molecules were readily obtained by vacuum deposition. Films that were vacuum deposited onto the substrate at room temperature resulted in more amorphous films than those spin coated.

The thermal properties, including melting and decomposition temperatures, of these molecules are shown in Table 1. Differential scanning calorimetry (DSC) was used to investigate phase transitions. No glass transitions or crystallization events were observed by DSC scans of the molecules. All the materials had melting transitions ranging from 268 to 380 °C, with hexyl substituted **1b** and **1e** melting at the lowest temperatures, 268 °C and 274 °C, respectively, and unsubstituted **1a** melting at the highest temperature, 380 °C. The decomposition temperatures determined by thermogravimetric analysis were between 406 °C and 451 °C, demonstrating that the series of diphenylanthrazolines **1a**−**1e** are very robust molecules.

X-ray Crystal Structures. Crystals were grown by slow evaporation of THF/methanol solutions. Single crystals from three of the five diphenylanthrazolines (**1b**, **1c**, and **1d**) were suitable for the determination of X-ray crystal structures. **1b** was obtained as thin orange prisms, and **1d** was obtained as thin yellow needles. Large orange prisms were obtained for **1c** resulting in excellent quality data. **1b** and **1d** were found to have primitive monoclinic crystal systems. A c-centered monoclinic C lattice was found for **1c**. The unit cell parameters of a = 14.2910(10) Å, b = 5.8370(4) Å, c = 21.752(2) Å, and β = 104.231(3)° for **1b**, a = 23.8400(8) Å, b = 5.6920(2) Å, c = 22.5290(10) Å, and β = 93.7610(12)° for **1c**, and a = 12.7580-(8) Å, b = 4.8680(6) Å, c = 21.476(2) Å, and β = 95.856(2)° for **1d** are reported for the molecules. The space groups were $P2_1/c$, $C2/c$, and $P2_1/c$ for **1b**, **1c**, and **1d**, respectively. Structures were refined to final residuals of R_1 = 6.57% for **1b**, R_1 = 3.50% for **1c**, and R_1 = 5.08% for **1d**. The detailed crystallographic data for **1b**, **1c**, and **1d** are collected in Table 2.

Table 2. Crystallographic Data for Diphenylanthrazolines **1b**, **1c**, and **1d**

	1b	**1c**	**1d**
formula	C48 H48 N2	C44 H38 N2	C38 H28 N2 O2
formula weight	652.88	594.76	544.62
crystal system	monoclinic	monoclinic	monoclinic
color of crystal	orange	orange	yellow
space group	$P2_1/c$ (no. 14)	$C2/c$ (no. 15)	$P2_1/c$ (no. 14)
a [Å]	14.2910 (10)	23.8400 (8)	12.7580 (8)
b [Å]	5.8370 (4)	5.9620 (2)	4.8680 (6)
c [Å]	21.752 (2)	22.5290 (10)	21.476 (2)
β (deg)	93.7610 (12)	104.231 (3)	95.856 (2)
volume [Å^3]	1758.8 (2)	3195.2 (2)	1326.8 (2)
temperature [K]	130	130	130
Z	2	4	2
R_f	0.0657	0.0350	0.0508
R_w	0.1825	0.0923	0.1332
GOF	1.018	1.051	0.933

The single crystal structures and packing diagrams of **1b** and **1c** are shown in Figures 1 and 2. In **1b** and **1c**, the pendant 4,9-diphenyl groups are twisted 68° and 58°, respectively, from the plane of the anthrazoline unit. These phenyl groups were found to be disordered in **1d**, resulting in 62° and 113° in a 1:2 ratio (Figure 3). The α-linked phenyl groups were twisted 4° in **1b**, 15° in **1c**, and 28° in **1d** from the plane of the anthrazoline unit. This indicates that the planarity of the molecules is increased by longer substituents on the α-linked phenyl group. The molecular packing of molecules **1b** and **1c** are very similar, whereas the packing of **1d** is more complex due to the disorder

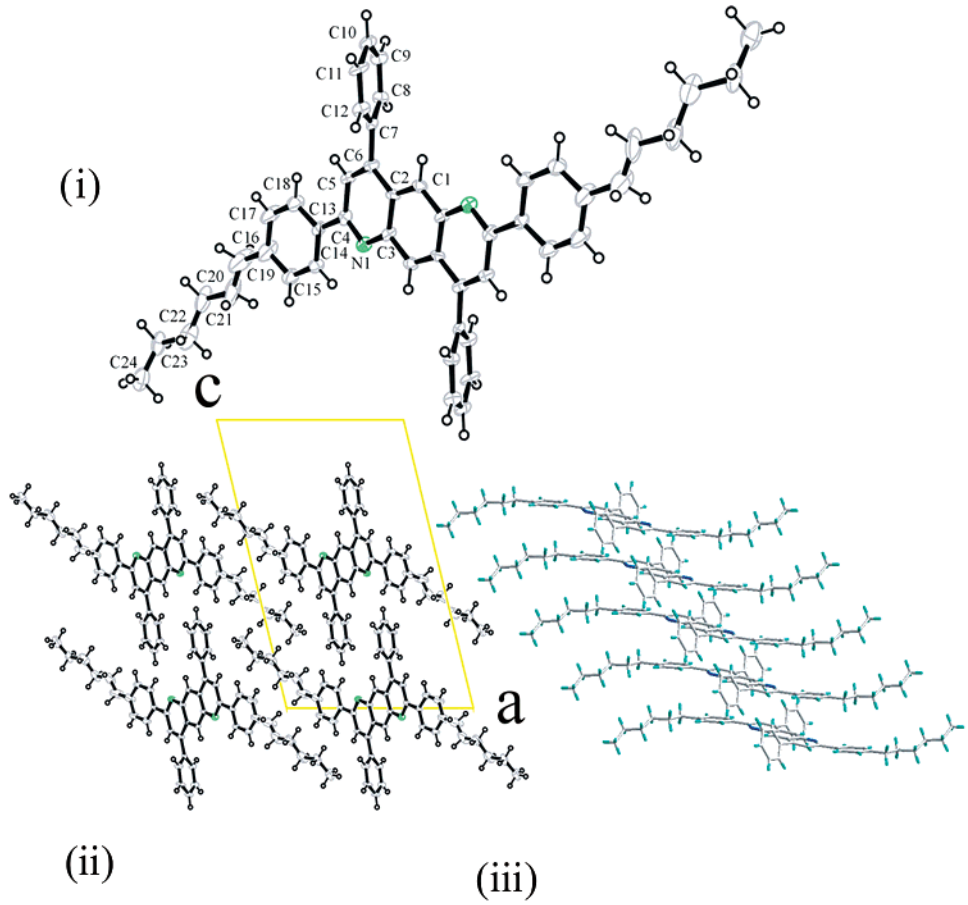

Figure 1. Single crystal structure of **1b** (i), view down the *b* axis (ii), and view down the *a* axis (iii).

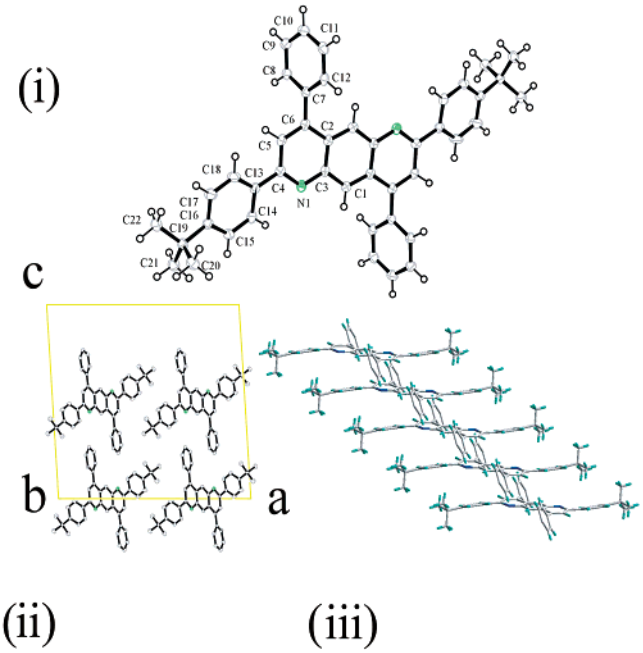

Figure 2. Single crystal structure of **1c** (i), view down the *b* axis (ii), and view down the *a* axis (iii).

of the pendant phenyl rings. Both **1b** and **1c** exhibit edge-to-face packing of the pendant phenyl rings to neighboring planar units (anthrazoline and the bis (α-linked phenyl) groups). Although the intermolecular distance between the faces of the anthrazoline rings in both **1b** and **1c** is ca. 3.40 Å, the anthrazoline units tend to stack themselves more uniformly in **1c**. The vertical alignment of the anthrazoline rings results in π-stacking of the pendant phenyl groups which are separated by a distance of 2.60 Å. Neighboring molecules of **1b** are shifted so that the anthrazoline unit is above the α-linked phenyl group. The intermolecular distance between planar anthrazoline units, ca. 3.9 Å, was much larger in **1d**. The disordered pendant phenyl rings in **1d** align themselves in an unparallel fashion away from the nearby methoxy groups, while still exhibiting edge-to-face π-stacking.

These single crystal structures of the diphenylanthrazolines provide a basis for elucidating the effect of solid-state morphology on their photophysics and charge transport properties. Also since these molecules are excellent model systems for the conjugated polyanthrazolines,[27] we expect the present X-ray crystal structures to shed light on the structural and physical properties of the high molecular weight polyanthrazolines. Single crystal structures of oligoquinolines have similarly provided valuable information as model systems for the conjugated polyquinolines.[28]

Electrochemical Properties. Cyclic voltammetry was done on solutions and thin films of all diphenylanthrazolines. The cyclic voltammograms (CVs) of the four soluble diphenylanthrazolines **1a**−**1d** are shown in Figure 4. All four molecules in solution clearly show reversibility of the reduction waves as evident from the areas and proximity of the anodic and cathodic

(28) Shetty, A. S.; Liu, E. B.; Lachicotte, R. L.; Jenekhe, S. A. *Chem. Mater.* **1999**, *11*, 2292−2295.

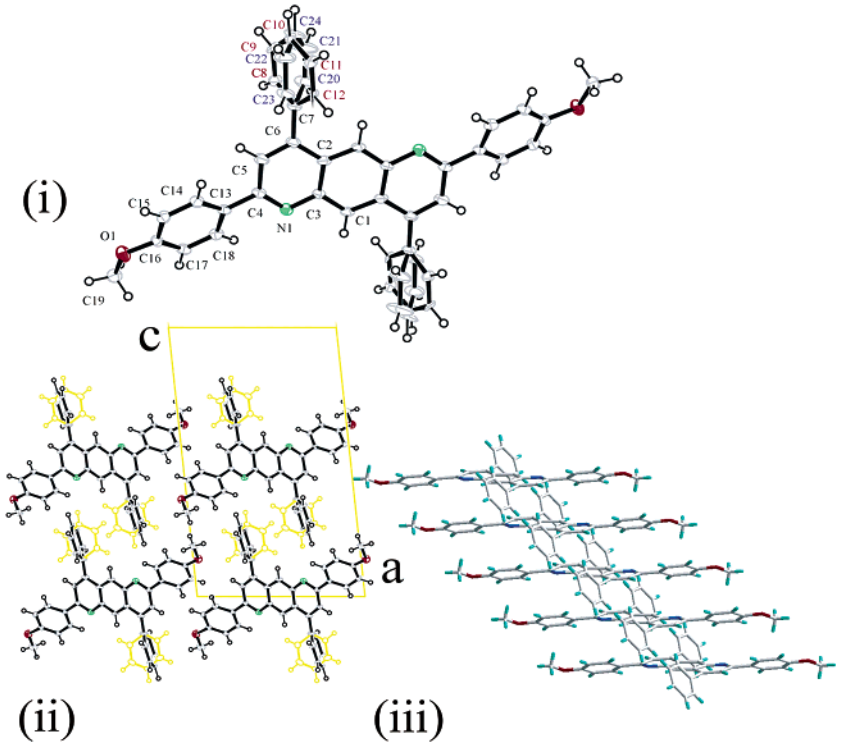

Figure 3. Single crystal structure of **1d** (i), view down the *b* axis (ii), and view down the *a* axis (iii).

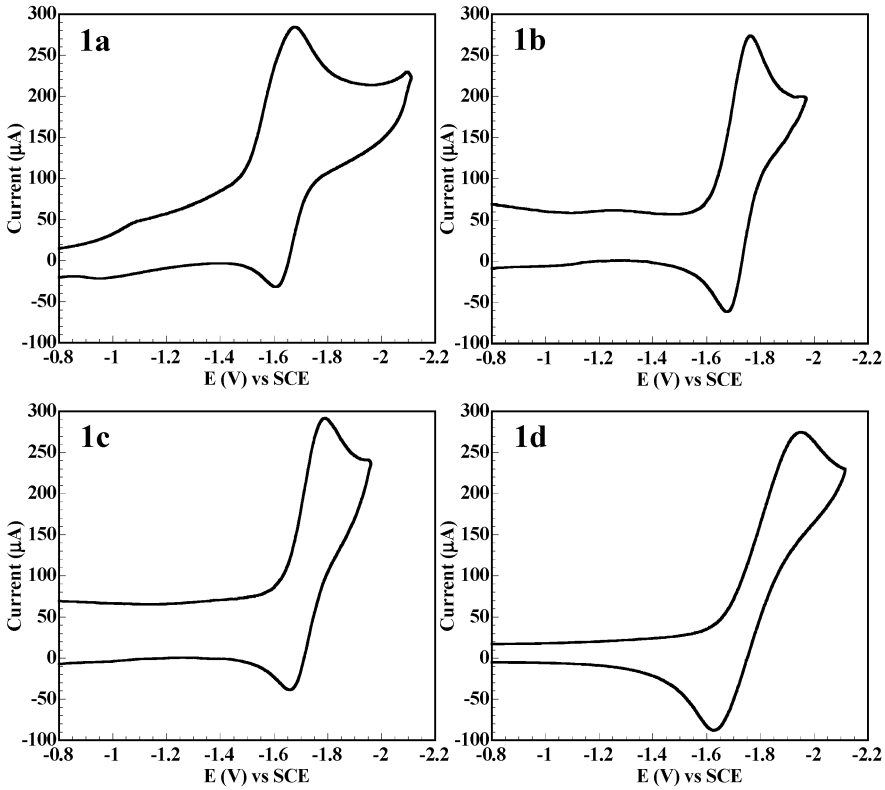

Figure 4. Cyclic voltammograms of compounds **1a**−**1d** (1−3 mM) in CH_2Cl_2/acetonitrile (7:3 v/v), 0.1 M $TBAPF_6$. Scan rate = 300 mV/s.

peaks. The half-wave reduction potential ($E_{1/2}$) of the molecules varies from −1.55 V (vs SCE) for **1e** to −1.78 V for **1d** (Table 3).

Typical CVs of the diphenylanthrazolines as thin films on electrodes are shown in Figure 5. The oxidation and reduction voltammograms for **1a** are shown in Figure 5a. A quasi-reversible reduction peak was seen when scanned to −1.6 V (the dotted line). Scanning to more negative potentials (the solid line) showed a second peak and loss of reversibility as the reduced molecule becomes soluble in the electrolyte. All five molecules display this quasi-reversible double reduction peak. The cyclic voltammogram of **1c** shows a larger second reduction peak while maintaining quasi-reversibility of the first peak (Figure 5b). Figure 5c shows the oxidation and reduction

Table 3. Electrochemical Properties of Diphenylanthrazolines in Solution[a,b]

compd	E_{pc}^{red} (V)	E_{pa}^{red} (V)	$E_{1/2}$ (V)
1a	−1.61	−1.67	−1.64
1b	−1.68	−1.76	−1.72
1c	−1.66	−1.78	−1.72
1d	−1.63	−1.94	−1.78
1e	−1.50	−1.59	−1.55

[a] All potentials vs SCE reference. [b] 1−3 mM in CH_2Cl_2/acetonitrile (7:3 v/v), 0.1 M $TBAPF_6$. Scan rate = 300 mV/s.

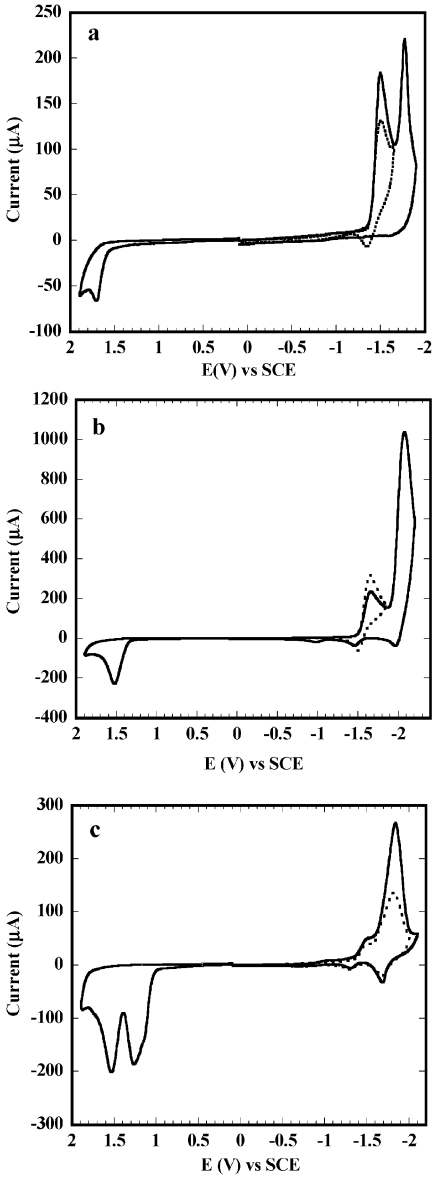

Figure 5. Cyclic voltammograms of thin films of **1a** (a), **1c** (b), and **1e** (c) coated on a Pt wire electrode. Scan rate = 40 mV/s.

voltammogram of **1e**. In addition to the quasi-reversible double reduction peak, an irreversible double oxidation peak is also observed for this molecule. All the other diphenylanthrazolines had one irreversible oxidation peak. These features of irreversible oxidation but quasi-reversible reduction have previously been observed in the diphenylanthrazoline polymers.[29] The

Table 4. Electrochemical Properties of Diphenylanthrazolines[a]

compd	$E_{red}^{\circ\prime}$ (V)	E_{red}^{onset} (V)	EA (eV)	E_{ox}^{peak} (V)	E_{ox}^{onset} (V)	IP (eV)	E_g^{el} (eV)
1a	−1.42	−1.30	3.10	1.70	1.45	5.85	2.75
1b	−1.48	−1.39	3.01	1.65	1.25	5.65	2.64
1c	−1.58	−1.50	2.90	1.52	1.25	5.65	2.75
1d	−1.53	−1.43	2.98	1.65	1.30	5.70	2.72
1e	−1.39	−1.40	3.00	1.20	0.95	5.35	2.35

[a] All potentials vs SCE reference.

observed reduced reversibility of the reduction waves in thin films compared to solution is also due in part to counterion diffusion limitations.

Table 4 shows the solid-state electrochemical data for **1a**−**1e**. HOMO and LUMO levels were estimated from the onset potentials by comparison to ferrocene (4.4 eV versus vacuum).[29] Electron affinities (LUMO levels) were estimated from the onset of the reduction wave (EA = E_{red}^{onset} + 4.4 eV). We note however that the oxidation potential of ferrocene has also been reported as −4.8 eV below vacuum.[30] All five diphenylanthrazolines have electron affinities between 2.90 and 3.10 eV (below vacuum). The reduction potentials of all the molecules are relatively unchanged by α-linked aryl groups, indicating that the LUMOs lie on the anthrazoline moiety. Even the electron-rich bithiophene substituted molecule (**1e**), which as expected has the lowest oxidation potential, has essentially the same LUMO level as the other four molecules.

The formal reduction potential ($E_{red}^{\circ\prime}$) varies from −1.39 V (vs SCE) for **1e** to −1.58 V for **1c** (Table 4). The electron-donating strength of the 2,7-substituents on the diphenylanthrazoline unit (R group) shifts the formal reduction potential to more negative values. In contrast, increasing the electron-donating strength of the R group shifts the first oxidation peak and onset oxidation potential to less positive values. As a result the estimated ionization potential (IP = E_{ox}^{onset} + 4.4 eV) is reduced from 5.85 eV in **1a** to 5.35 eV in **1e**. Also shown in Table 4 are the electrochemically derived band gap (E_g^{el}) of thin films of the diphenylanthrazolines. The band gap varies from 2.75 eV for **1a** and **1c** to 2.35 eV for **1e**. The electrochemical band gap is smallest in **1e** as expected from the large delocalization length facilitated by the bithiophene R groups.

Comparison of the $E_{red}^{\circ\prime}$ values of the diphenylanthrazolines to other nitrogen heterocycles is shown in Chart 2 confirms the expected progression of reduction potential and thus electron affinity. The average $E_{red}^{\circ\prime}$ value of **1a**−**1e**, −1.45 ± 0.10 V, falls between acridine (V) and phenazine (VI). This average reduction potential of **1a**−**1e** is also significantly more positive compared to those of oxadiazole (X) and benzothiadiazole (IX), both which have been widely explored as building blocks for electron-transport materials for organic LEDs.[1e,2a,3b,10,17] On the other hand, the average $E_{red}^{\circ\prime}$ of the diphenylanthrazolines is significantly less positive than that of pyrazinoquinoxaline (VII) which has a reduction potential of −0.96 V. These results demonstrate that model heterocycle information can be used to predict properties of new materials incorporating the heterocycles. The formal reduction potentials for **1a**−**1e** also suggest that organic semiconductors with even higher electron affinities can be achieved by incorporating more imine nitrogens in the basic building blocks.

(29) (a) Agrawal, A. K.; Jenekhe, S. A. *Chem. Mater*. **1996**, *8*, 579−589. (b) Yang, C. J.; Jenekhe, S. A. *Macromolecules* **1995**, *28*, 1180−1196. (c) Alam, M. M.; Jenekhe, S. A. *J. Phys. Chem. B* **2002**, *106*, 11172−11177.

(30) (a) Jegou, G.; Jenekhe, S. A. *Macromolecules* **2001**, *34*, 7926−7928. (b) Stuve, E. M.; Krasnopoler, A.; Sauer, D. E. *Surf. Sci*. **1995**, *335*, 177−185

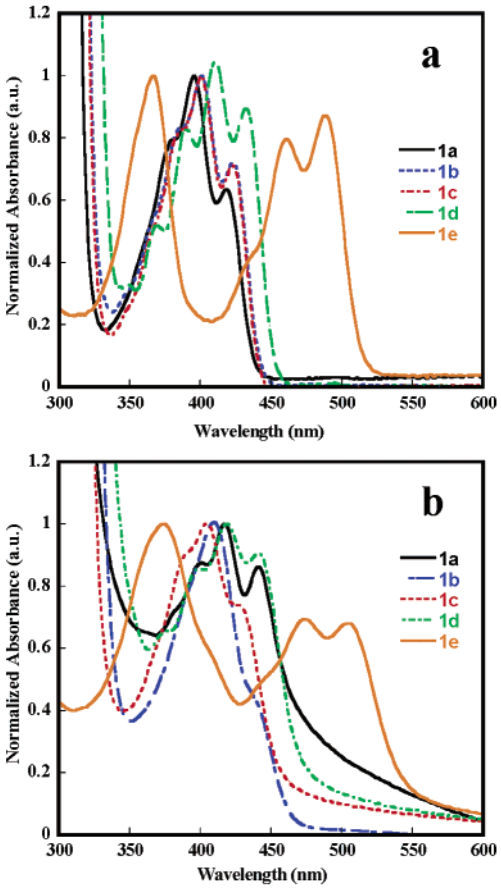

Figure 6. Optical absorption spectra of **1a**−**1e** in toluene solution (a) and solid state (b).

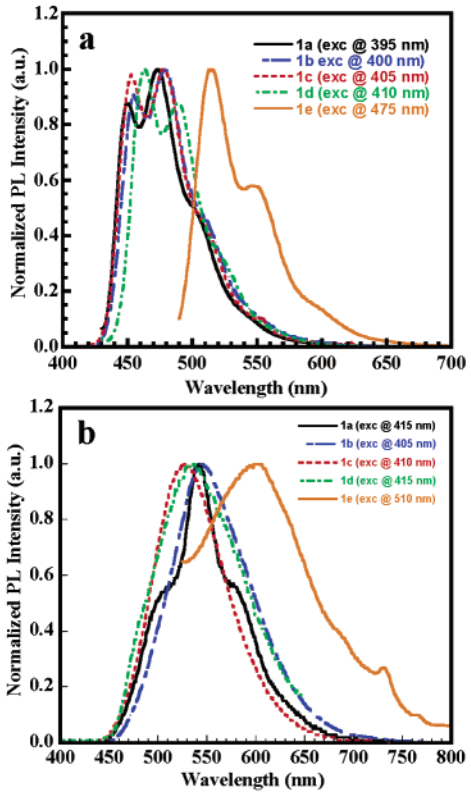

Figure 7. PL spectra of **1a**−**1e** in toluene solution (a) and solid state (b).

Photophysical Properties. Absorption spectra of all five diphenylanthrazolines in toluene solution are shown in Figure 6a. The lowest energy absorption bands are from the $\pi-\pi^*$ transitions by virtue of their large molar extinction coefficients ($\epsilon \approx 10^4-10^5$ M^{-1} cm^{-1}). All the solution absorption spectra of **1a**−**1e** are structured. Unsubstituted **1a** and alkyl substituted **1b** and **1c** have nearly identical absorption maxima (λ_{max}) at 399, 395, and 400 nm, respectively. Alkoxy substituted **1d** has absorption λ_{max} that is red shifted 12 nm compared to **1a** as a result of the electron-donating methoxy moiety. The increase in conjugation length and the increased electron density associated with the bithiophene groups lead to a large bathochromic shift of absorption maximum in **1e** to 488 nm. For all the diphenylanthrazoline compounds except **1e**, the absorption λ_{max} corresponds to the 0−1 optical transition. Although the 0−0 transition in these four compounds (**1a**−**1d**) is a distinct peak, its oscillator strength is smaller than the 0−1 transition (absorption maximum). In the case of **1e**, the lowest energy transition is identical with the 0−0 optical transition; we believe that this arises from the greater molecular planarity and π-electron delocalization in **1e** compared to the other compounds. There is an additional absorption band in the 300−400 nm range with a maximum at 366 nm ($\epsilon = 8.0 \times 10^4$ M^{-1} cm^{-1}). The exact origin of the additional absorption band is unclear. It is no doubt a consequence of the block co-oligomer architecture of **1e** as similar absorption features have previously been observed in donor−acceptor conjugated alternating co-polymers and model compounds.[31] The 366-nm band in the absorption spectrum of **1e** in solution is likely due to the optical transitions localized on the bithiophene chromophores.

The solid-state optical absorption spectra of compounds **1a**−**1e** are shown in Figure 6b. The structured absorption bands observed in solution are also seen in the solid state. The solid-state absorption bands are, however, red shifted by about 3−4 nm in **1c** and **1d** and 14−16 nm in **1a**, **1b**, and **1e** compared to their corresponding ones in solution. The similarity of the solution and the solid-state absorption spectral line shape in these molecules suggest that there is a slight increase in conjugation length in the solid state, accounting for the 3−16 nm red shift in absorption maximum. Such an increase in conjugation length is expected from the more planar conformations due to the π-stacking in the solid state as observed in the X-ray single-crystal structures. Optical band gaps (E_g^{opt}) determined from the absorption edge of the solid-state spectra are given in Table 1. The optical band gap varies from 2.21 eV in **1e** to 2.70 eV in **1a**. These values are in good agreement with those determined from cyclic voltammetry (Table 4).

The dilute solution (10^{-5} M) photoluminescence (PL) spectra of **1a**−**1e** are shown in Figure 7a. All five compounds have structured emission bands. In the case of **1a**−**1d**, they emit blue light with the emission maximum in the 462−482-nm range. If the 0−0 transitions in the emission and corresponding absorption bands are considered, the Stokes shift is small for all the compounds. In dilute solutions of **1e**, green PL emission is observed with an emission maximum of 524 nm. The PL quantum yield (ϕ_f) of compounds **1a**−**1e** in dilute solution in

(31) (a) Lai, R. Y.; Fabrizio, E. F.; Lu, L.; Jenekhe, S. A.; Bard, A. J. *J. Am. Chem. Soc.* **2001**, *123*, 9112−9118. (b) Jenekhe, S. A.; Lu, L.; Alam, M. M. *Macromolecules* **2001**, *34*, 7315−7324.

toluene was relatively high, ranging from 58% for **1e** to 76% for **1c** (Table 1). The fluorescence quantum efficiencies of **1a**−**1d** are very similar at 68−76%, whereas that of **1e** is significantly lower. The lower emission quantum yield in **1e** is due in large part to the donor−acceptor−donor nature of this diphenylanthrazoline and consequent intramolecular charge transfer which is known to be an important luminescence quenching mechanism in such donor−acceptor systems.[31b]

The PL emission spectra of the thin films of **1a**−**1e** are shown in Figure 7b. In addition to their broad featureless characteristics, these solid-state emission bands are significantly red shifted from the dilute solution ones. The similarities of the dilute solution and solid-state absorption spectra and the emission spectral features in conjunction with the π-stacking of the molecules in the solid state suggest that excimer emission[32] best describes the thin film luminescence of **1a**−**1e**. Consistent with this interpretation is the finding that the estimated relative PL quantum yield in the thin films was in the 20−30% range for **1a**−**1d** and only 3% for **1e** (Table 1). The especially poor PL emission efficiency in thin films of **1e** is also in accord with the strong intramolecular charge-transfer character of **1e** compared to the other diphenylanthrazolines.

A comparison of the solid-state photophysical properties of diphenylanthrazolines **1b**, **1c**, and **1d**, for which single crystal structures were attained, appears to suggest a trend between molecular planarity and the Stokes shift. The observed Stokes shift of the molecules follows the trend **1b** (136 nm) > **1c** (123 nm) > **1d** (120 nm). This correlates well to the trend in torsion angle between the α-linked phenyl group and the anthrazoline unit, i.e., the planarity of the molecule: **1b** (4°) > **1c** (15°) > **1d** (28°). It is to be expected that the planarity of the molecule dictates the degree of intermolecular interaction and thus excimer formation.[32]

Light-Emitting Diode Properties. We explored diphenylanthrazolines **1a**−**1e** in light-emitting diodes (LEDs) both as the emissive and as electron-transport (n-type) materials. The intrinsic electroluminescence (EL) of these compounds is first presented and discussed. To investigate the EL properties of **1b**−**1e**, we fabricated LEDs using poly(ethylenedioxythiophene)/poly(styrene sulfonic acid) (PEDOT) thin film on indium tin oxide (ITO) as the anode, the spin-coated diphenylanthrazoline as the emissive layer, and aluminum as the cathode: ITO/PEDOT/**1b**−**1e**/Al. The EL spectra of **1a**−**1e** are shown in Figure 8a. The broad structureless line shapes of the EL spectra are similar to those of the PL spectra (Figure 7b) and are indicative of excimer emission. The EL spectra are nearly identical to the respective PL spectra with the exception of **1b**. The EL spectrum of the most planar **1b** shows a large red shift in emission maximum compared to the other diphenylanthrazolines. The red shift in the electroluminescence spectrum of **1b** relative to the PL spectrum is likely due to more efficient π-stacking and increased order at the internal operating temperatures of the LEDs. The device characteristics of LEDs of the type ITO/PEDOT/**1a**−**1e**/Al are shown in Table 5. The turn-on voltage (electric field) of these diodes was 5−16 V ((8−20) × 10^5 V/cm). The maximum brightness of the devices was 7−82 cd/m^2 for **1a**−**1e** as emissive materials. The corresponding external quantum efficiency (EQE) was also low, 0.002−0.045% (Table 5).

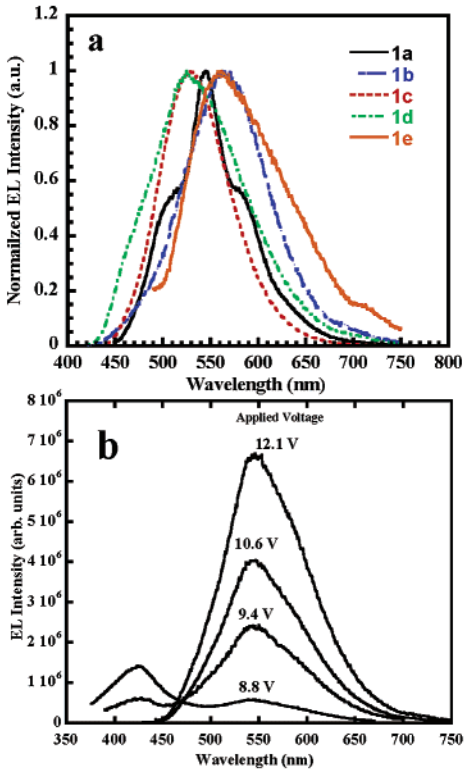

Figure 8. EL spectra of **1a**−**1e** (a) and ITO/PEDOT/PVK/**1b**/Al diode (b).

Table 5. Electroluminescent Device Properties of Diphenylanthrazolines

LED configuration[a]	turn-on voltage, V	maximum brightness, cd/m^2 (V_{max})[b]	current maximum, mA/cm^2	EQE, %	power efficiency, lm/W	device efficiency, cd/A
MEH-PPV	4	53	500	0.06		
1a	16	7	124	0.002		
1b	14	32 (20)	135	0.006		
1c	7.5	82 (14)	174	0.045		
1d	5	46 (8)	306	0.040		
1e	6.5	27 (11)	500	0.008		
PVK/**1b**	8	122 (13)	200	0.06		
PVK/**1d**	8	133 (13)	229	0.07		
MEH-PPV/**1a**	7	690 (18)	43	1.3	0.3	1.8
MEH-PPV/**1b**	7	595 (18)	15	3.1	2.0	7.0
MEH-PPV/**1c**	7	579 (20)	14.5	2.9	0.9	5.0
MEH-PPV/**1d**	6	965 (17)	116	1.1	0.2	0.8
MEH-PPV/**1e**	10	468 (18)	44	0.6	0.2	1.1

[a] ITO/PEDOT/MEH-PPV/Al, ITO/PEDOT/**1**/Al, ITO/PEDOT/PVK/**1b**(or **1d**)/Al, and ITO/PEDOT/MEH-PPV/**1**/Al. [b] Brightness at maximum bias voltage.

The energy levels of compounds **1a**−**1e** are shown in Figure 9a along with those of other materials and the LED electrode materials. It appears that the rather poor performance of **1a**−**1e** as emissive materials in LEDs is likely due to the large barrier (~0.8−1.3 eV) for hole injection from PEDOT into **1a**−**1e**. We confirmed this in part by inserting a poly(*N*-vinylcarbazole) (PVK) layer between the PEDOT and **1b** or **1d** in LEDs. Figure 8b shows the EL spectra of one such diode, ITO/PEDOT/PVK/**1b**/Al. The observed EL emission is green, primarily from **1b**. At 8.8 V, a weak blue emission from the PVK layer is also observed as a peak at ca. 430 nm. This blue emission is not

(32) (a) Jenekhe, S. A.; Osaheni, J. A. *Science* **1994**, *265*, 765−768. (b) Osaheni, J. A.; Jenekhe, S. A. *Macromolecules* **1994**, *27*, 739−742.

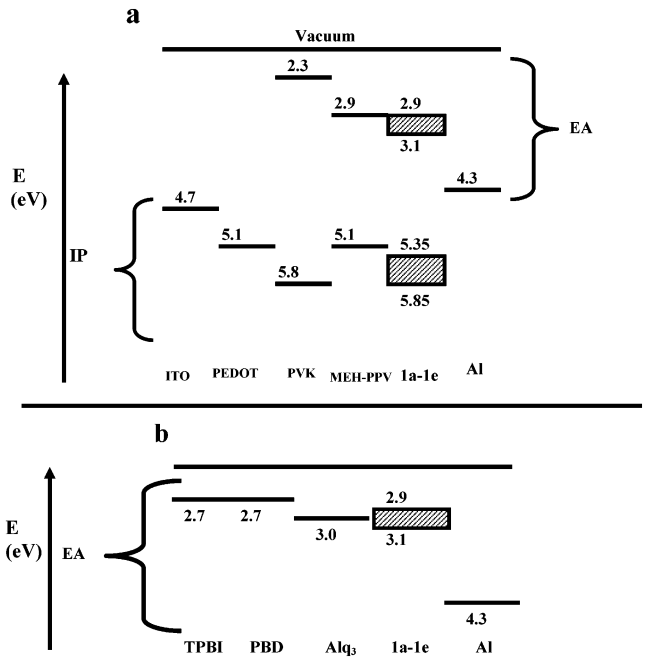

Figure 9. Energy diagrams of LED materials (a) and other n-type molecules (b).

observed at voltages greater than 10 V when only the peak at ca. 550 nm is seen.

These devices showed improvement in both brightness and efficiency as shown in Table 5. Brightness and external quantum efficiency values nearly doubled to 133 cd/m^2 and 0.07%. The rather large ionization potential (IP) of the diphenylanthrazolines and thus hole blocking properties in combination with their high electron affinities (EA) suggest that they are probably more promising as electron-transport (n-type) materials in organic and polymer LEDs than as emissive materials. In this respect, we note that the electron affinity values of **1a**−**1e** are much larger than those of commonly used current electron-transport materials Alq_3,[16] 2-(4-biphenylyl)-5-(4-*tert*-butylphenyl)-1,3,4-oxadiazole (PBD),[17] and 2,2′,2″-(1,3,5-benzenetriyl)tris[1-phenyl-1*H*-benzimidazole] (TPBI)[18] as shown in Figure 9b.

We evaluated the diphenylanthrazolines **1a**−**1e** as electron-transport materials in polymer LEDs by using poly(2-methoxy-5-(2′-ethyl-hexyloxy)-1,4-phenylene vinylene) (MEH-PPV) as the emissive material. The bilayer LEDs ITO/PEDOT/MEH-PPV/**1a**−**1e**/Al were fabricated by spin coating of the MEH-PPV layer followed by vacuum evaporation of compounds **1a**−**1e** at 3×10^{-6} Torr. The film thickness of **1a**−**1e** as electron-transport layers in these diodes was in the range 60 to 65 nm. The typical EL spectra from these bilayer LEDs are exemplified in Figure 10 for the ITO/PEDOT/MEH-PPV/**1d**/Al diode. At all applied bias voltages in this and other bilayer diodes, only the characteristic orange-red emission of MEH-PPV with an EL emission maximum at 569 nm was seen, demonstrating that **1a**−**1e** functioned as electron-transport materials.

The current−voltage and luminance−voltage characteristics of the MEH-PPV diodes using **1a**−**1e** as electron-transport materials are shown in Figure 11. The associated LED performance information is collected in Table 5. The turn-on voltage of these LEDs was about 6−10 V (∼1.3×10^6 V/cm). The maximum brightness of the LEDs was in the range of 468 cd/m^2 for **1e** to 923 cd/m^2 for **1d**. However, in terms of the external

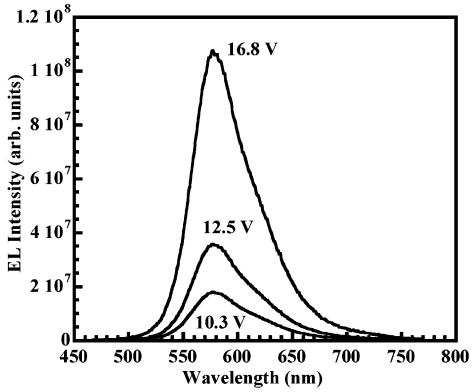

Figure 10. EL spectra of ITO/PEDOT/MEH-PPV/**1d**/Al diode.

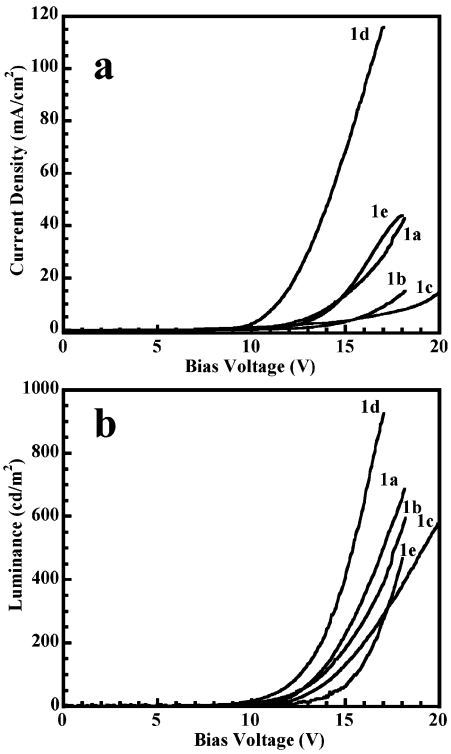

Figure 11. Current−voltage curves (a) and current−luminance curves (b) for all five LEDs using **1a**−**1e** as the electron-transport layer and MEH-PPV as the emissive layer.

quantum efficiency (EQE), power efficiency (lm/W), and device efficiency (cd/A), **1b** was the best electron-transport material, with 3.1% EQE, 2.0 lm/W, and 7.0 cd/A. The overall performance of the series of compounds as electron-transport materials in MEH-PPV LEDs was in the decreasing order **1b** > **1c** > **1a** > **1d** > **1e**. There are no obvious molecular structure factors, electrochemical properties, or crystallographic features of the series of molecules **1a**−**1e** that correlate with this observed trend. Although it is intriguing that the two best electron-transport materials among the series, **1b** and **1c**, are the most planar based on the crystal structures, there is no evidence that such planarity is maintained in the largely amorphous vacuum deposited films.

There is much evidence in the literature for the use of electron-transport materials to improve the device performance of organic and polymer LEDs, of special interest here, arylene vinylene polymer based LEDs.[1a,4e,f,h,10] Both polymers, such as polypyridines[20c] and polyquinolines,[21c] and small molecules,

such as Alq_3[33] and oxadiazoles,[17a] have been used as the electron-transport materials in MEH-PPV LEDs. The best reported performance of such bilayer devices was external quantum efficiencies of up to 0.24%.[20c] Our group has also used several n-type polymers in this capacity. For examples, the n-type polymers poly(2,2′-(3,3′-dioctyl-2,2′bithienylene)-6,6′-bis(4-phenylenequinoline))[4f] and poly(*p*-phenylene benzobisthiazole)[4h] as electron-transport layers for MEH-PPV diodes gave efficiencies of 0.76 and 2.5%, respectively. The present results on diodes of the type ITO/PEDOT/MEH-PPV/**1a**−**1e**/Al thus show that the new diphenylanthrazolines **1a**−**1e** are superior electron-transport materials for polymer LEDs.

Conclusions

We have synthesized and investigated the electrochemical, photophysical, electroluminescent, and electron-transport properties of a new family of useful electron-transport (n-type) materials based on the 4,9-diphenylanthrazoline core. Single crystal X-ray structures of three of the diphenylanthrazolines (**1b**, **1c**, and **1d**) showed that they crystallized in the monoclinic system with the space groups $P2_1/c$, $C2/c$, and $P2_1/c$, respectively, and different unit cell parameters. The 2,7-linked phenyl groups were twisted 4°−15° from the plane of the anthrazoline unit in **1b**−**1c**, demonstrating the high degree of planarity of the molecules. The high electron affinities of the new compounds (2.90−3.10 eV) together with their robust thermal stability suggested that they have promising electron-transport properties for organic LEDs. Initial use of the diphenylanthrazolines **1a**−**1e** as the electron-transport materials in bilayer MEH-PPV LEDs showed substantial enhancement in device performance under ambient air conditions (3.1% external quantum efficiency, 2.0 lm/W, 965 cd/m^2), and thus superior performance, compared to most current electron-transport materials for LEDs. As derivatives of anthracene, which is known to exhibit high carrier mobilities (∼1−2 cm^2/Vs at 300 K) in molecular crystals,[34] we expect that further modification could also make the diphenylanthrazolines suitable materials for n-channel thin film transistors.

Experimental Section

Materials. 4′-*n*-Hexylacetophenone was purchased from TCI. All other reagents were purchased from Aldrich and used as received.

Synthetic Procedures. 2,5-Dibenzoyl-1,4-phenylenediamine[35] and 5-*n*-hexyl-2,2′-bithiophene[36] were synthesized according to known literature methods.

5-Acetyl-5′-*n*-hexyl-2,2′-bithiophene. To a solution of 1.51 g of 5-*n*-hexyl-2,2′-bithiophene in 50 mL of anhydrous CH_2Cl_2 was added a stirred solution of 0.80 g of acetic anhydride in 150 mL of anhydrous CH_2Cl_2 followed by a solution of 3.5 g of $SnCl_4$ in 150 mL of anhydrous acetonitrile. The mixture was stirred at room temperature for 24 h under argon atmosphere and then poured over crushed ice containing 50 mL of AcOH. The organic layer was separated, and the aqueous layer was extracted with 2 × 100 mL of CH_2Cl_2. The combined organic layer was washed with 10% NaOH aqueous solution and H_2O and dried with $MgSO_4$, and the solvent was removed to yield brown oil. Purification on a silica gel column with 1:1 CH_2Cl_2/hexanes yielded 0.91 g of the desired product as a light brown oil (53% yield). ^{1}H NMR ($CDCl_3$): δ ppm 7.70 (s, 1H), 7.22 (dd, 2H), 6.91 (d, 1H), 2.83 (t, 2H), 2.64 (s, 3H), 1.71 (t, 2H), 1.34 (m, 6H), 0.93 (t, 3H). Calcd for $C_{16}H_{20}OS_2$: C, 65.71; H, 6.89; S, 21.93. Found: C, 65.78; H, 6.64; S, 21.65.

General Procedure for Synthesis of 1a−1e. 2,5-Dibenzoyl-1,4-phenylenediamine (1 equiv), acetyl-functionalized compound (2.2 equiv), diphenyl phosphate (5 g), and toluene (5 mL) were added to a dry reaction flask. The flask was purged with argon for 20 min, and the temperature was gradually raised to 120 °C and stirred for 24 h. The reaction mixture was precipitated into 10% triethylamine/ethanol and collected by vacuum filtration. The precipitate was passed through a silica gel column via flash chromatography to remove impurities. The resulting product was then recrystallized from tetrahydrofuran/methanol solutions ranging from 2 to 20% MeOH. Each was recrystallized twice.

2,7-Bis(phenyl)-4,9-diphenylanthrazoline (1a). Yield was 62% as orange crystals; mp 380 °C. ^{1}H NMR ($CDCl_3$): δ ppm 8.89 (s, 2H), 8.24 (d, 4H), 7.90 (s, 2H), 7.73 (d, 4H), 7.64 (m, 6H), 7.55 (t, 4H, 7.51 (t, 2H). FTIR (KBr, cm^{-1}): 1587, 1520, 1469, 1421, 1181, 1005, 876, 838, 825, 760. HRMS (FAB) calcd for $C_{36}H_{25}N_2$ 485.20177, found 485.20216.

2,7-Bis(4′-*n*-hexylphenyl)-4,9-diphenylanthrazoline (1b). Yield was 72% as yellow-orange needles; mp 274 °C. ^{1}H NMR ($CDCl_3$): δ ppm 8.85 (s, 2H), 8.15 (d, 4H), 7.87 (s, 2H), 7.72 (d, 4H), 7.64 (m, 6H), 7.36 (d, 4H), 2.71 (t, 4H), 1.68 (q, 4H), 1.34 (m, 12H), 0.91 (t, 6H). ^{13}C NMR ($CDCl_3$): δ ppm 158.67, 157.09, 154.00, 149.55, 145.36, 139.15, 135.93, 130.21, 127.41, 126.78, 122.43, 33.26, 31.05, 30.08, 29.60, 23.01, 14.42. FTIR (KBr, cm^{-1}): 2921, 2851, 1592, 1570, 1535, 1490, 1454, 1351, 1184, 1018, 884, 836, 770. HRMS (FAB) calcd for $C_{48}H_{49}N_2$ 653.38957, found 653.38824.

2,7-Bis(4′-*tert*-butylphenyl)-4,9-diphenylanthrazoline (1c). Yield was 71% as yellow-orange needles; mp 356 °C. ^{1}H NMR ($CDCl_3$): δ ppm 8.86 (s, 2H), 8.15 (d, 4H), 7.88 (s, 2H), 7.73 (d, 4H), 7.64 (m, 6H), 7.57 (t, 4H), 1.40 (s, 18H). ^{13}C NMR ($CDCl_3$): δ ppm 158.29, 157.16, 153.50, 149.68, 146.66, 138.75, 136.70, 130.09, 127.39, 126.23, 120.35, 35.22, 31.68. FTIR (KBr, cm^{-1}): 2965, 2857, 1585, 1563, 1558, 1534, 1495, 1358, 1154, 1005, 886. HRMS (FAB) calcd for $C_{44}H_{41}N_2$ 597.32697, found 597.32691.

2,7-Bis(4′-methoxyphenyl)-4,9-diphenylanthrazoline (1d). Yield was 78% as yellow needles; mp 347 °C. ^{1}H NMR ($CDCl_3$): δ ppm 8.80 (s, 2H), 8.21 (d, 4H), 7.85 (s, 2H), 7.71 (d, 4H), 7.71−7.65 (m, 6H), 7.06 (d, 4H), 3.91 (s, 6H). ^{13}C NMR ($CDCl_3$): δ ppm 159.88, 157.67, 154.00, 148.98, 146.80, 138.55, 136.78, 129.31, 127.90, 125.88, 120.55, 65.08. FTIR (KBr, cm^{-1}): 2995, 2983, 1591, 1565, 1479, 1466, 1426, 1339, 1247, 1105, 1050, 1005, 887, 790. HRMS (FAB) calcd for $C_{38}H_{29}N_2O_2$ 545.2229, found 545.22312.

2,7-Bis(5′-*n*-hexyl-2,2′-bithiophene)-4,9-diphenylanthrazoline (1e). Yield was 68% as red powder; mp 268 °C. ^{1}H NMR ($CDCl_3$): δ ppm 8.63 (s, 2H), 7.73 (s, 2H), 7.64 (m, 10H), 7.16 (dd, 4H), 6.74 (d, 2H), 2.83 (t, 4H), 1.71 (t, 4H), 1.34 (m, 12H), 0.93 (t, 6H). FTIR (CCl_4, cm^{-1}): 2960, 2926, 2852, 1734, 1604, 1591, 1575, 1490, 1479, 1465, 1432, 1368, 1330, 1261, 1097, 1059, 1017, 918, 907. HRMS (FAB) calcd for $C_{52}H_{49}N_2S_4$ 829.27786, found 829.27851.

General. ^{1}H NMR and ^{13}C NMR spectra were recorded on a Bruker DRX-499 spectrometer at 499 MHz using $CDCl_3$ as the solvent. Fourier transformation infrared (FTIR) spectroscopy was done either by a solution cell technique using CCl_4 or as a film on a KBr plate using a Perkin-Elmer 1720 FT-IR spectrometer. Thermogravimetric analysis of the molecules was conducted on a TA Instruments Q50 TGA. A heating rate of 10 °C/min under flowing N_2 was used with runs being conducted from room temperature to 600 °C.

Photophysics. Optical absorption spectra were obtained by using a Lambda-900 UV/vis/near-IR spectrophotometer (Perkin-Elmer). Photoluminescence spectra were carried out on a PTI QuantaMaster model QM-2001-4 spectrofluorometer (Photon Technology International Inc. Ontario, Canada).

(33) Kim, K.; Lee, D. W.; Jin, J. L. *Synth. Met.* **2000**, *114*, 49−56.
(34) Pope, M.; Swenberg, C. E. *Electronic Processes in Organic Crystals and Polymers*; Oxford University Press: New York, 1999; pp 337−339.
(35) Stille, J. K.; Kurihara, M.; Katto, T.; Johnson, E. F.; Imai, Y. *J. Polym. Sci.* **1975**, *13*, 2233−2248.
(36) Barbarella, G.; Favaretto, L.; Sotgui, G.; Zambianchi, M.; Antolini, L.; Pudova, O.; Bongini, A. *J. Org. Chem.* **1998**, *63*, 5497−550.

Cyclic Voltammetry. Cyclic voltammetry experiments were done on an EG&G Princeton Applied Research Potentiostat/Galvanostat (model 273A). Data were collected and analyzed by the model 270 Electrochemical Analysis System Software on a PC computer. A three-electrode cell was used in all experiments as previously described.[29] Platinum wire electrodes were used as both counter and working electrodes, and silver/silver ion (Ag in 0.1 M $AgNO_3$ solution, Bioanalytical System, Inc.) was used as a reference electrode. A ferrocene/ferrocenium (Fc/Fc^+) redox couple was used as an internal standard, and the potential values, thus, obtained in reference to the Ag/Ag^+ electrode were converted to the saturated calomel electrode (SCE) scale. Solution cyclic voltammetry was carried out in a mixed CH_2CL_2/acetonitrile (7:3 v/v) solvent containing $TBAPF_6$ (0.1 M) as an electrolyte for all compounds **1a**−**1e** with concentrations in the range 1−3 mM. All solutions in the three-electrode cell were purged with ultrahigh-purity N_2 for 10−15 min before each experiment, and a blanket of N_2 was used during the experiment. For solid-state cyclic voltammetry, the films of **1a**−**1e** were coated on the Pt working electrode by dipping the Pt wire into the viscous solution in chloroform and then drying it in a vacuum oven at 80 °C for 8 h. An electrolyte solution of 0.1 M $TBAPF_6$ in acetonitrile was used in all experiments keeping other conditions the same.

Fabrication and Characterization of LEDs. Three types of LEDs were fabricated and evaluated: ITO/PEDOT/**1a**−**1e**/Al, and ITO/PEDOT/PVK/**1b**(**1d**)/Al, and ITO/PEDOT/MEH-PPV/**1a**−**1e**/Al. Sequential spin coating of the layers onto a pre-cleaned ITO-coated glass substrate was used to fabricate the first two types. A thin layer of poly(ethylenedioxythiophene)-polystyrenesulfonate (PEDOT) (∼ 40 nm) was first spin coated from its solution in water onto ITO and dried at 80 °C in a vacuum for 12 h. For ITO/PEDOT/**1a**−**1e**/Al devices, thin films of **1a**−**1e** were spin coated from 1.0 wt % solutions in $CHCl_3$ onto the PEDOT layer and dried at 80 °C in a vacuum for 10 h. For ITO/PEDOT/PVK/**1b**(**1d**)/Al devices, PVK thin film was spin coated from a 0.5 wt % solution in $CHCl_3$ onto the PEDOT layer and dried at 50 °C in a vacuum for 10 h. In the case of ITO/PEDOT/MEH-PPV/**1a**−**1e**/Al devices, the MEH-PPV thin film was spin coated from a 0.5 wt % solution in $CHCl_3$ onto the PEDOT layer and dried at 50 °C in a vacuum for 10 h. The diphenylanthrazolines **1a**−**1e** were then each vacuum deposited onto the MEH-PPV thin film using an Edwards Auto 306 vacuum evaporator at pressures of ca. 3×10^{-6} Torr. The multilayer thin films were dried in a vacuum at 80 °C for 10 h before deposition of the aluminum electrode under vacuum (3×10^{-6} Torr). A 100-nm thick aluminum layer was thermally deposited to form active diode areas of 0.2 cm^2 (5-mm diameter).

The film thickness was measured by using an Alpha step profilometer (model 500, KLA-Tencor, San Jose, CA), which has a resolution of ±1 nm. Electroluminescence (EL) spectra were measured on a PTI spectrofluorometer. The electrical characteristics of the devices were measured (model 211) on an HP4155A semiconductor parameter analyzer together with a Grasby S370 optometer equipped with a calibrated luminance sensor head. The EL quantum efficiencies of the diodes were measured by using the procedures similar to those previously reported.[4c] All the fabrications and measurements were done under ambient laboratory conditions.

Acknowledgment. This research was supported by the U.S. Army Research Laboratory and the U.S. Army Research Office under the TOPS MURI program (Grant DAAD19-01-1-0676), the Air Force Office of Scientific Research (Grant F49620-03-1-0162), and in part by the Office of Naval Research and the Boeing−Martin Professorship Endowment.

Supporting Information Available: ^1H NMR spectra and thermogravimetric analysis curves of all compounds. This material is available free of charge via the Internet at http://pubs.acs.org.

JA036314E